

PEGASE: a UV to NIR spectral evolution model of galaxies

Application to the calibration of bright galaxy counts

Michel Fioc¹ and Brigitte Rocca-Volmerange^{1,2}

¹ Institut d'Astrophysique de Paris, CNRS, 98 bis Bd. Arago, F-75014 Paris, France

² Institut d'Astrophysique Spatiale, Bât. 121, Université Paris XI, F-91405 Orsay, France

Received ??; accepted ??

Abstract. PEGASE (Projet d'Etude des GALaxies par Synthèse Evolutive, in French) is a new spectrophotometric evolution model for starbursts and evolved galaxies of the Hubble sequence. Its main originality is the extension to the near-infrared (NIR) of the atlas of synthetic spectra of Rocca-Volmerange & Guiderdoni (1988) with a revised stellar library including cold star parameters and stellar tracks extended to the thermally-pulsing regime of the asymptotic giant branch (TP-AGB) and the post-AGB (PAGB) phase. The NIR is coherently linked to the visible and the ultraviolet (UV), so that the model is continuous on an exceptionally large wavelength range from 220 Å up to 5 μm. Moreover, a precise algorithm allows to follow very rapid evolutionary phases such as red supergiants or AGB crucial in the NIR. The nebular component is also computed in the NIR. The extinction correction is gas-dependent for spirals and ellipticals. A set of reference synthetic spectra at $z = 0$, to which apply cosmological k - and evolution e - corrections for high-redshift galaxies, is built from fits of observational templates. Because of the lack of visible to NIR spectral templates for each Hubble type, we adopt statistical samples of colors, not fitted by previous models.

A first application of this continuous model is to solve the problem of the slope of the bright galaxy counts from $B = 15$ to 19 and of the normalization parameter ϕ_* of the Schechter luminosity function.

Designed to be used currently and to take into account easily new observational and theoretical inputs, the model is built as a series of independent blocks. Any block is clearly identified and submitted to publication. Code sources, input and output data are available¹ by anony-

mous ftp at [ftp.iap.fr](ftp://ftp.iap.fr/pub/from_users/pegase/) in `/pub/from_users/pegase/` or at the WEB address of the authors: <http://www.iap.fr/users/>.

Key words: Galaxies: evolution – Infrared: galaxies – dust, extinction – Galaxies: stellar content – Cosmology: miscellaneous – Galaxies: fundamental parameters

1. Introduction

The recent development of NIR observational astronomy, as well as the progress of the theory of stellar evolution (overshooting, nuclear rates, winds, opacities, see Maeder & Meynet (1989); Chiosi (1986)), notably of the evolved phases (Groenewegen & de Jong 1993; Vassiliadis & Wood 1993) up to the PAGB terminal phases (Blöcker 1995), put new constraints on the evolution of galaxies. The UV-optical range of currently star-forming galaxies is dominated by young stars, and results of models limited to this domain are unable to determine the past star formation history. To break this degeneracy, the NIR emission of the bulk of giants is worthy to be examined as a meaningful indicator of mass and age. Moreover, the NIR light is less obscured by dust than at shorter wavelengths and has proved very useful in the spectral analysis of dusty starbursts (Lançon et Rocca-Volmerange 1996). Following star formation history over a long timescale thus needs a continuity of the wavelength range. That continuity is also necessary to analyze distant galaxies at large redshift ranges in the deepest galaxy counts. From the long series of models compared by Arimoto (1996) and Charlot (1996) at the Crete meeting, most current models agree in the visible. However, none of them is published in the NIR by Leitherer et al. (1996a), possibly because they show a flux deficit from J to K in the spectral energy distribution (SED) of early-type galaxies (Arimoto 1996).

Send offprint requests to: M. Fioc, e-mail: fioc@iap.fr

¹ A first version is in the AAS CD-ROM Series, vol. 7 (Leitherer et al. 1996b)

The poor knowledge of the atmospheric parameters of cold stars dominating the NIR and the rapid evolution of the latest phases are evident difficulties for the modeling of NIR emission. Another difficulty is the connection of the NIR stellar emission to the visible at about $1 \mu\text{m}$, where cold stars of $T_{\text{eff}} \simeq 2000$ to 3000 K peak. Moreover, in that domain, only a few data are available because receivers in the optical as in the NIR have minimal sensitivity.

Our main goal is to build a new atlas of evolving standard synthetic spectra for the types of the Hubble sequence. We present here UV to NIR energy distributions for 8 spectral galaxy types. Evolutionary parameters are constrained by fitting synthetic spectra at $z = 0$ on integrated spectra and colors of nearby galaxies. The choice of templates requires a peculiar attention to aperture effects and a significant identification of Hubble types. These criteria have led us to use statistical color samples, because of the lack of significant spectral templates in the NIR wavelength range. The samples of optical and NIR data show however a high dispersion, which is partly observational, but is also due to uneven star formation histories leading to an intrinsic scatter of colors for a given morphological type. This makes it difficult to identify observational templates.

A first application of PEGASE solves the puzzling question of the bright galaxy counts. The slope at bright magnitudes is shown to be in agreement with recent *multispectral* observations of Gardner et al. (1996), excluding the strong evolution of giant galaxies at low redshift advocated by Maddox et al. (1990) from their steep counts. Moreover, the normalization of the luminosity function is in accordance with the high value of Marzke et al. (1994).

The structure of this paper is as follows. In section 2, we present our model, the algorithm, the stellar library and other related data, the evolutionary tracks, the nebular emission and finally the extinction model. In section 3, we examine the star formation history for starbursts and evolved galaxies and propose evolutionary scenarios fitted on UV to NIR observations of galaxies of the Hubble sequence. In section 4, we check that the evolution of our standard scenario is realistic by comparison with bright galaxy counts, and we finally discuss in the conclusion the advantages and limitations of the model.

2. The model

The two historical models of Tinsley (1972) and Searle et al. (1973) computed, respectively, the photometric evolution of galaxies from isomass stellar evolutionary tracks and isochrones. When applied to the same stellar evolutionary model and with similar input data (stellar spectra library, bolometric corrections...), both methods should give equivalent results, so that output differences must arise from deficient algorithms. Refined algorithms recently improved to conserve the released energy and the stability of outputs without suffering any degradation by

smoothing methods are presented here. The stellar library is improved in the visible and the UV and is coherently extended by using NIR spectra and colors of stars on a significant cover of the HR diagram. Evolutionary tracks of the Geneva and Padova groups may be used up to the beginning of thermal pulses and are completed with stellar models of the final phases up to the PAGB phase. The nebular emission, computed as in Guiderdoni & Rocca-Volmerange (1987) (hereafter GRV), is extended to the NIR and a new modeling of extinction in elliptical galaxies is proposed.

2.1. The integration algorithm

Although the principle of spectral evolutionary synthesis is simple, computational problems and erroneous results may be caused by unoptimized algorithms. The monochromatic flux of a galaxy at age t and wavelength λ may be written

$$F_{\lambda}(t) = \int_0^t \int_{m_1}^{m_u} \tau(t-\theta) \phi(m) f_{\lambda}(m, \theta) dm d\theta,$$

where $\tau(t-\theta)$ is the star formation rate (SFR) at time $t-\theta$ in M_{\odot} per time and mass units, $\phi(m)$ the initial mass function (IMF) defined in the interval $[m_1, m_u]$ and normalized to $1 M_{\odot}$, and $f_{\lambda}(m, \theta)$ the monochromatic flux of a star with initial mass m at wavelength λ and at age θ since the zero age main sequence (ZAMS) (null if θ exceeds the lifetime duration). A simple discretization of both integrals leads however to oscillations of the emitted light (Charlot & Bruzual 1991). Mainly due to the rapid evolutionary phases such as TP-AGB or massive red supergiants, they can be solved with a sufficient time resolution requiring substantial computer times (Lançon & Rocca-Volmerange 1996). In fact, oscillations are observed at any time t that a stellar population of mass m moves off from a stellar phase before the subsequent population of mass $m + \delta m$ reaches the same evolutionary phase. Resulting oscillations present a real difficulty in simulating instantaneous bursts, while they are artificially smoothed with continuous star formation laws. To avoid that problem, one possibility is to discretize only one of the two integrals. For example (isomass method, discretization of the integral on mass):

$$F_{\lambda}(t) = \sum_{i=1}^{p-1} \tau(t-\theta_i) \sum_{j=1}^{q-1} \phi(m_j) (m_{j+1} - m_j) \times \int_{\theta_i}^{\theta_{i+1}} f_{\lambda}(m_j, \theta) d\theta$$

where $\theta_1 = 0$, $\theta_p = t$, $m_1 = m_l$, $m_q = m_u$ and $m_{j+1} - m_j$ is sufficiently small that equivalent phases of consecutive masses overlap. An alternative is to discretize the other integral on time (isochrone method):

$$F_{\lambda}(t) = \sum_{i=1}^{p-1} \tau(t-\theta_i) (\theta_{i+1} - \theta_i) \int_{m_1}^{m_u} \phi(m) f_{\lambda}(m, \theta_i) dm$$

with $\theta_{i+1} - \theta_i$ short enough, so that consecutive isochrones $\int_{m_1}^{m_u} \phi(m) f_\lambda(m, \theta_i) dm$ have evolved little. Both algorithms have been checked by us to give identical results. In the following, we prefer, unlike in our previous models, the isochrone method partly because isochrones are directly comparable to color-magnitude diagrams of star clusters and also for computational reasons.

2.2. Stellar spectra and calibrations

2.2.1. The stellar library

Although the libraries of synthetic stellar spectra become more and more reliable, the physics of the cold stars dominating in the NIR (1 μm to 5 μm), notably the blanketing effects that lead to color temperatures very different to the effective ones (Lançon & Rocca-Volmerange 1992), is at the moment not taken sufficiently into account to build synthetic spectra of galaxies. For this reason, as in our previous models, we prefer to adopt observational libraries when possible and synthetic spectra otherwise. After reduction of various photometric systems to the Glass filters, standard optical and infrared colors were derived by Bessel & Brett (1988) for stars later than B8V and G0III. We have used these colors to derive fluxes at mean wavelengths of the infrared filters for the stars of our UV-optical library and fitted cubic splines to these fluxes. Hotter star spectra are extended in the NIR with a blackbody at T_{eff} . The color temperatures derived in Lançon & Rocca-Volmerange (1992) could be used instead, but it should make no significant difference since, at these temperatures the blackbody is used in the Rayleigh-Jeans wavelength range. A stellar library observed with a better resolution in the NIR with the FTS/CFHT is in preparation. In the mid-infrared ($\lambda > 5 \mu\text{m}$), we use the analytic extension of Engelke (1992) for stars colder than 6000 K. For M giants, which strongly dominate in the NIR, we use the spectra of Fluks et al. (1994) with the temperatures they provide. Their good resolution in spectral types is essential since $V - K$ increases very rapidly with decreasing temperature.

The library from the far-UV to the NIR respects the effective temperature of any spectral type all along the wavelength range. Anomalous stellar spectra and wrong identifications of spectral types in the published libraries may produce erroneous colors and spectra of galaxies. For this reason, optical spectra were selected from the library of Gunn & Stryker (1983) according to the following procedure: $(B - V, U - B)$, $(B - V, V - R_c)$ and $(B - V, R_c - I_c)$ color-color diagrams for all the stars of the library were plotted. Least square polynomials were fitted to the points, and we only selected stars in good agreement with the fits. Effective temperatures were derived from $B - V$ according to the calibration from Straižys (1992), except for M dwarfs, the temperatures of which were calculated from $R_c - I_c$ according to Bessel (1995). In the

far-UV (1230-3200 Å), stellar spectra are extracted from the IUE ESA/NASA libraries (Heck et al. 1984) and, after correction for extinction with the standard law of Savage & Mathis (1979), connected to the visible. E_{B-V} is computed from the observed $B - V$ taken from Lanz (1986) or Wesselius et al. (1982) and the $(B - V)_0$ corresponding to the spectral type from Straižys (1992). Anomalous spectra near 2000 Å (especially O stars) due to the bump of the extinction curve have been eliminated, as well as those in strong disagreement with the slope of the UV continuum of Kurucz (1992) for the corresponding temperature. In the extreme-UV (220-1230 Å), we complete our spectra with Kurucz (1992) models for $T_{\text{eff}} < 50\,000$ K. The models of Clegg & Middlemass (1987) are finally used at all wavelengths for stars hotter than 50 000 K. Our stellar library is available in the AAS CD-ROM or on our anonymous account.

2.2.2. Bolometric corrections

We compute the bolometric corrections from Fluks et al. (1994) spectra for M giants (getting thus a coherent set of spectra, temperatures and bolometric corrections), and adopt those given by Bessel (1995) for late-M dwarfs, Vacca et al. (1996) for very hot stars or else the values tabulated by Straižys (1992). The bolometric corrections that we compute from our spectra, since only a negligible flux should be emitted outside our wavelength range, are in good agreement with the above values from the literature, making us confident that our identification in T_{eff} is correct and that the junctions between the UV, optical and NIR domains are valid.

2.3. Evolutionary tracks

Stars are followed from the ZAMS to the final phases (supernovae or white dwarfs according to their masses), including the TP-AGB, fundamental to model NIR spectra, and PAGB phases. To check the sensitivity of spectral synthesis to evolutionary tracks, we compare the solar metallicity tracks of Bressan et al. (1993) (hereafter “Padova”) to those of Schaller et al. (1992) extended by Charbonnel et al. (1996) (hereafter “Geneva”). The “Padova” tracks overshoot for masses $m \geq 1 M_\odot$ and use a higher ratio of the overshooting distance to the pressure scale height and down to lower masses than Geneva tracks, which include overshooting above 1.5 M_\odot only. Both sets use the OPAL opacities (Iglesias et al. 92), similar mixing lengths, helium contents (0.28 for Padova and 0.30 for Geneva) and mass loss rates. We do not consider other metallicities, since these tracks already lead to significant discrepancies (see 3.1.1) which make the comparison of observed and synthetic spectra uncertain. Both sets go up to the beginning of the TP-AGB for intermediate and low-mass stars and have been prolonged by TP-AGB using typical luminosities and evolutionary timescales from Groenewegen

& de Jong (1993) for stars less massive than $6 M_{\odot}$. The PAGB models of Schönberner (1983) and Blöcker (1995), supported by observations of planetary nebulae (Tylenda & Stasińska 1994), are finally connected to the tracks.

Whatever the algorithm used, interpolation between tracks requires the identification of the corresponding points. The interpolation algorithm adopted here aims to conserve the released energy along any track. For Padova models, sets of evident equivalent points are selected on consecutive mass tracks. Considering now such points A_i and A_j of track A and the corresponding ones B_p and B_q of track B , we may build a new track B' replacing track B with $B'_i = B_p$ and $B'_j = B_q$. Intermediate points B'_k are computed iteratively so that $E_{B'}(k, k+1)/E_{B'}(i, j) = E_A(k, k+1)/E_A(i, j)$, where $E(u, v)$ is the energy emitted from u to v . Equivalent points are given for Geneva tracks except in the interval $[1.7 - 2] M_{\odot}$, for which the previous procedure has been used. For low mass stars, we use the tracks of Vandenberg et al. (1983). Except when otherwise stated, we use Padova tracks with their complements to the latest phases and to low mass stars, because of their higher resolution in mass and time and because Geneva tracks may not be interpolated after 16 Gyr, since post-helium flash evolution is not available in the $0.8 M_{\odot}$ track.

2.4. Nebular emission

Gaseous nebulae are assumed to be optically thick in Lyman lines, according to case B recombination, the most likely for isolated nebulae (Osterbrock 1989). As in our previous models, the ratio of line intensities in the hydrogen recombination spectrum is computed for a given set of electronic temperature and density ($T_e = 10\,000$ K, $n_e = 1 \text{ cm}^{-3}$) of astrophysical interest. In the NIR, the Paschen and Brackett lines were computed, relative to Balmer lines, by Pengelly (1963) and Giles (1977). Other emission lines such as H_2 ($2.12 \mu\text{m}$), He I ($2.06 \mu\text{m}$) and [Fe I] ($1.6 \mu\text{m}$), detected in NIR spectra of galaxies, were added in a ratio observed in typical starbursts (Lançon & Rocca-Volmerange 1996). Main lines of starbursts were also added, following Spinoglio & Malkan (1992).

The nebular continuum emission coefficients in the infrared are taken from Ferland (1980) for H I and He II. H I coefficients may be used instead of He I in the NIR (Ferland 1995). Two-photon emission coefficients are taken from Brown & Mathews (1970) but are negligible in the NIR.

The number of ionizing photons is a fraction f of the number of Lyman continuum photons computed from our spectral library, while the rest is assumed to be absorbed by dust. We take $f = 0.7$, in agreement with the values obtained by DeGioia-Eastwood (1992) for H II regions in the LMC.

2.5. Extinction

The extinction by dust which affects the SED of galaxies depends on the spatial distribution of dust and stars and on its composition, narrowly related to the metallicity Z of the ISM. The optical depth τ_{λ} is related as in GRV to the column density of hydrogen N_{H} and the metallicity.

The metallicity evolution $Z(t)$ is computed from Woosley & Weaver (1995) SNII models without the instantaneous recycling approximation. Since the extinction is described as a function of the global metallicity, we neglect the yields of SNIa and intermediate and low mass stars. Models A are used for initial masses $m \leq 25 M_{\odot}$ and B for $m \geq 30 M_{\odot}$ following Timmes et al. (1995). From ($Z = 0.001$) and ($Z = 0.02$) Woosley & Weaver (1995) models, we may approximate the net yield m_Z in solar masses as follows:

$$\begin{aligned} m_Z &= 0 && \text{if } m/M_{\odot} \leq 10.2 \\ m_Z &= 0.223m - 2.27 && \text{if } 10.2 \leq m/M_{\odot} \leq 18.8 \\ m_Z &= 0.401m - 5.62 && \text{if } 18.8 \leq m/M_{\odot} \leq 30.9 \\ m_Z &= 8.96 \cdot 10^{-2}m + 4 && \text{if } 30.9 \leq m/M_{\odot}. \end{aligned}$$

Dust effects may be approximated in the simplest cases of the phase function, respectively isotropy and forward-scattering. Calzetti et al. (1994) proposed to model scattering effects, with a combination of isotropic and forward-only scattering accounting for anisotropy, for mixed dust and sources by replacing τ_{λ} by the following effective depth

$$\tau_{\text{eff}}(\lambda) = (h_{\lambda}(1 - \omega_{\lambda})^{1/2} + (1 - h_{\lambda})(1 - \omega_{\lambda}))\tau_{\lambda},$$

where the albedo ω_{λ} is from Natta & Panagia (1984), and the weight parameter h_{λ} is derived by the authors from a Henyey-Greenstein phase function. We adopt their expression instead of the one of GRV, which corresponds to the case $h_{\lambda} = 1$.

The geometry for the disk extinction is modelled by a uniform plane-parallel slab as in GRV. The resulting face-on optical depth for Sa-Sc spirals at 13 Gyr is about 0.55 in the B -band. Assuming the same geometry, Wang & Heckman (1996) deduced the face-on optical depth of a sample of disks from far-UV to far-infrared ratio and found $\tau_{\text{B}} = \tau_{\text{B}}^*(L_{\text{B}}/L_{\text{B}}^*)^{0.5 \pm 0.2}$, where L_{B}^* is the classical Schechter parameter of luminosity functions and $\tau_{\text{B}}^* = 0.8 \pm 0.3$ the corresponding depth, in good agreement with our values.

To model the extinction in spheroids, we must specify the distribution of stars and dust. Since it is more appropriate to describe the inner regions of ellipticals, which are the more affected by extinction, we prefer to use a King model for stars rather than a de Vaucouleurs profile. The distribution of dust in spheroids is poorly known. Fröhlich (1982) proposed to describe the density of dust as a power of the density of stars: $\rho_{\text{dust}} \propto \rho_{\text{stars}}^n$, and found $n \sim 1/2$ for two ellipticals of the Coma cluster. Witt et al. (1992) and Wise & Silva (1996) suggest $n \sim 1/3$. Values $n \geq 1$

would lead to strong color gradients in ellipticals that are not observed (Silva & Wise 1996). Tsai & Mathews (1995) obtain from the X-ray profile of three ellipticals that the distribution of gas is proportional to the square root of the starlight profile. Assuming a constant dust to gas ratio in these galaxies, we find once again $n = 1/2$. We keep this value in the following and estimate the amount of extinction for the parameters of the model (b) of Tsai & Mathews (1995) which corresponds to a L_B^* galaxy. We finally suppose that the galaxy geometry has not changed with time. Introducing the core radius r_c and the outer radius r_t , the light density at a distance r from the center is

$$\rho_L(r) = \rho_0(1 + (r/r_c)^2)^{-3/2}$$

if $r < r_t$ and 0 otherwise. The ratio of the dust dimmed global flux F of the spheroidal galaxy to the direct flux F_0 is

$$F/F_0 = \frac{\int_0^{r_t} 2\pi R (\int_{-z_t}^{z_t} \rho_L(r) \exp(-\tau(R, z)) dz) dR}{\int_0^{r_t} 2\pi R (\int_{-z_t}^{z_t} \rho_L(r) dz) dR}$$

where z and R are the cylindrical coordinates, $z_t = (r_t^2 - R^2)^{1/2}$, $r = (R^2 + z^2)^{1/2}$ and $\tau(R, z) = \int_z^{z_t} k(1 + (R^2 + \zeta^2)/r_c^2)^{-3n/2} d\zeta$. k is computed from the central optical depth $\tau_c = \tau(0, -r_t)$ derived from the central column density of hydrogen $N_H(0)$. At any radius, we have

$$N_H(R) = K \int_{-z_t}^{z_t} (1 + (R^2 + z^2)/r_c^2)^{-3n/2} dz,$$

where K is derived from the total mass of hydrogen M_H of the galaxy. For a helium mass fraction of 28 % in the interstellar medium, we have

$$M_H = g(t)M_T/1.4 = \int_0^{r_t} 2\pi R m_H N_H(R) dR,$$

where $g(t)$ is the gas fraction, M_T the initial mass of gas of the galaxy and m_H the mass of the hydrogen atom. We finally obtain for the parameters of the model (b) of Tsai & Mathews (1995)

$$N_H(0) = 4.7 \cdot 10^{23} g(t) \text{ atoms.cm}^{-2}.$$

Although the central optical depth may be very high in the early phases of evolution of spheroidal galaxies, the extinction of the overall galaxy is only about 0.4 magnitudes in the B -band at maximum and is negligible nowadays. Since neither the geometry of stars and dust, nor the quantities and properties of dust in past E/S0 are known, the previous calculations should be considered simply as a reasonable attempt to give an order of magnitude of the effect of extinction in these galaxies.

3. The star formation history of galaxies

Scenarios of galaxy evolution aim to reproduce the spectral energy distribution of each galaxy type on the most extended wavelength range. The first step is to compute the evolving SED of an instantaneous burst of star formation for a given IMF. The evolution of a real galaxy may then be described by the convolution of an SFR, related for example to the gas content, and of instantaneous bursts of various ages.

3.1. Instantaneous burst

3.1.1. Weight of the evolutionary tracks

As shown by Charlot et al. (1996) from the comparison of the models of Bertelli et al. (1994), Worthey (1994) and Bruzual & Charlot (1996), discrepancies in the evolutionary tracks are the main sources of uncertainty in spectral synthesis. Instantaneous bursts are particularly suitable to test the weight of different evolutionary tracks on spectral synthesis, since spectra and colors are not

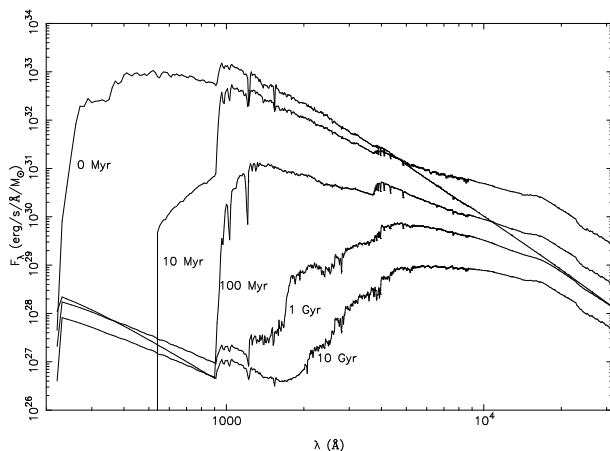


Fig. 1. Spectral evolution of an instantaneous burst of $1 M_\odot$. Nebular emission and extinction are not considered here.

smoothed by convolution with the SFR. In what follows, we use the polynomial form of the IMF obtained by Rana & Basu (1992), which accounts for the multiplicity of stars in the solar neighborhood. The slope of massive stars ($m \geq 6 M_\odot$) $x \sim -1.7$ corresponds to the value adopted in our previous models. Energy distributions of an instantaneous starburst from 200 Å to $3 \mu\text{m}$ are plotted at various ages in Fig. 1.

We show on Fig. 2 the evolution of the bolometric luminosity with time for the tracks of Padova and Geneva. The evolution is very similar for both sets up to 1 Gyr, where the low mass stars of the Padova set ($m \leq 2 M_\odot$) undergo the helium flash and provoke a bump in the bolometric luminosity. This bump is due to a flattening of the

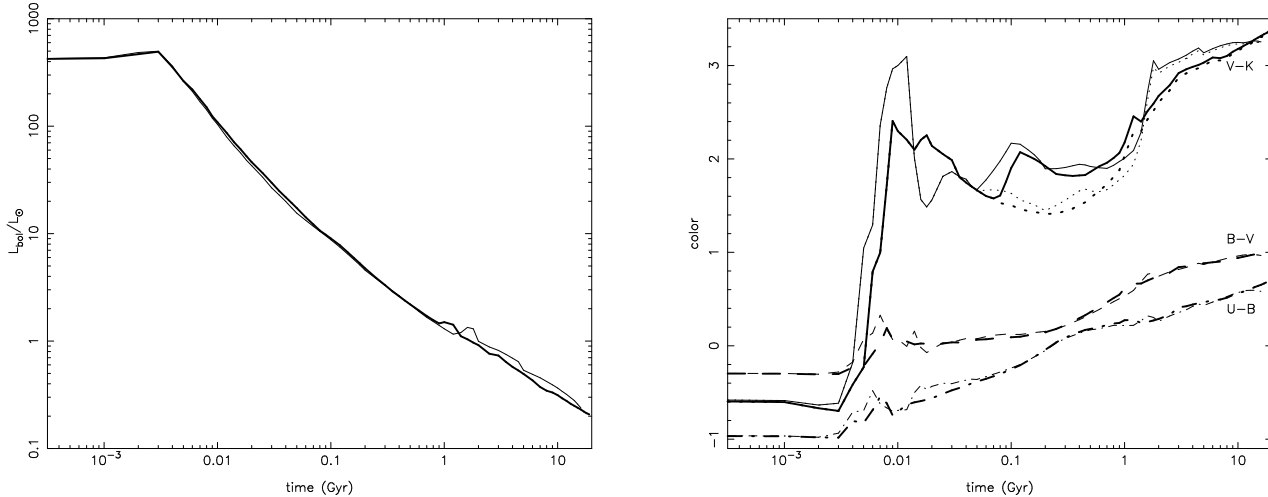


Fig. 2. Evolution of the bolometric luminosity (left) and colors (right) of an instantaneous burst. Thick lines are for Padova tracks and thin ones for Geneva. Solid: $V - K$, dashed: $B - V$, dash-dot-dash-dot: $U - B$. The weight of thermal pulses is observed on the $V - K$ curves computed without TP-AGB (dots).

stellar lifetime slope as a function of the initial mass of the stars in the interval $[2 - 2.2] M_{\odot}$. A similar feature is obtained at 1.8 Gyr, when the $1.7 M_{\odot}$ of the Geneva set also attains the helium flash. The luminosity of the burst computed with Geneva tracks is systematically about 15% higher after 2 Gyr than that of Padova, maybe because of overshooting. More striking differences may be observed on colors (see Fig. 2). Colors of the instantaneous star-burst are derived from convolution of the energy distributions through filter passbands and calibration on the Kurucz (1992) model of Vega. Massive stars of Geneva leave the ZAMS earlier than those of Padova but, whereas the subsequent evolution of $U - B$ and $B - V$ colors is similar, presumably because of the adjustment of the stellar evolutionary parameters on optical color-magnitude diagrams of star clusters, $V - K$ differs by as much as 0.9 magnitude at 12 Myr and 0.75 at 18 Myr. Different treatments of the red supergiant phase are clearly responsible for this, as shown by the isochrones at 12 and 18 Myr (see Fig. 3). While the 12 Myr isochrone of Geneva does not show any blue loop after the crossing of the HR diagram and is therefore redder than that of Padova, the 18 Myr isochrone extends to much higher temperatures and gives bluer colors. The color $V - K$ then evolves very slowly after 30 Myr, and both sets of tracks are in good agreement up to the helium flash where the bump observed in the bolometric luminosity is also visible. Geneva $V - K$ then exceeds the value of Padova by ~ 0.2 mag up to 13 Gyr, where curves cross one another. The $U - B$, $B - V$ and $V - K$ colors of Geneva then show a flattening trend or a blueing, the reason of which is unclear.

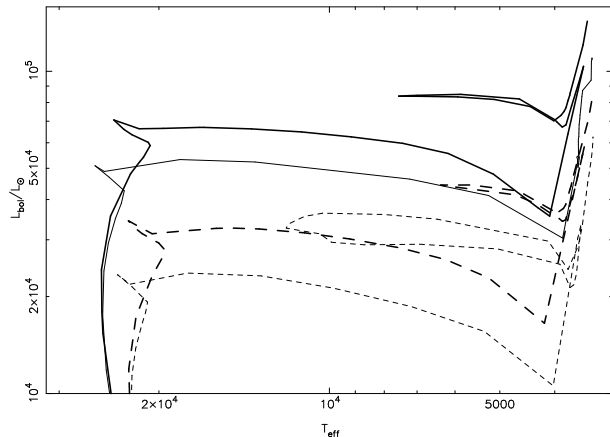


Fig. 3. Isochrones at 12 Myr (solid) and 18 Myr (dashed) of Padova tracks (thick) and Geneva tracks (thin).

Although the evolution of TP-AGB is poorly known, we show on Fig. 2 that the high-mass ($2 - 7 M_{\odot}$) TP-AGB stars may not be neglected and strongly redden the $V - K$ by as much as 0.6 mag at 100 Myr. The weight of TP-AGB becomes negligible after 2 Gyr and is insignificant at all ages for optical colors. Color-magnitude diagrams of optical-NIR colors should help to reduce the discrepancies between the tracks and to reduce the uncertainties on the evolution of red supergiants, but also on the phases following the helium flash.

3.1.2. Weight of the nebular emission

As shown in Fig. 4, the inclusion of nebular emission leads

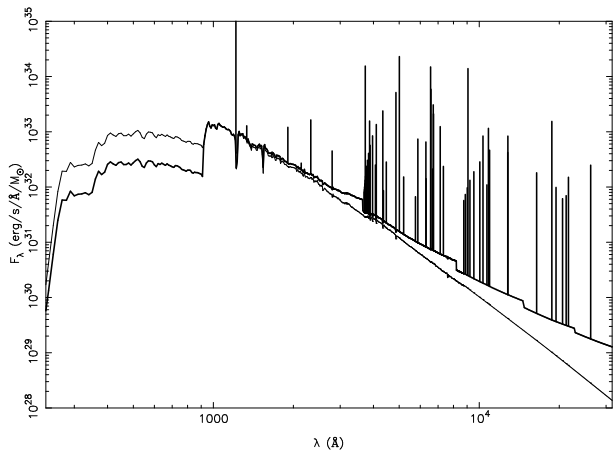


Fig. 4. Comparison of the spectra of an instantaneous burst at initial time with nebular emission (thick) and without (thin). 70% of Lyman continuum photons ionize the gas and lack shortward of 912 Å in the spectrum with nebular emission.

to prominent features, emission lines and discontinuities of the nebular continuum, which may not be neglected in the spectrum of an early instantaneous burst. To quantify the relative effect of the nebular component, in particular in the NIR, Table 1 gives the initial fraction of burst light through various filters, due to stars, lines and nebular continuum, respectively.

λ	stars	nebular continuum	emission lines
<i>U</i>	39.6	56.2	4.2
<i>B</i>	47.9	34.1	18.0
<i>V</i>	32.4	63.7	3.9
<i>R_c</i>	20.9	44.5	34.6
<i>I_c</i>	43.0	56.9	0.1
<i>J</i>	24.2	75.7	0.1
<i>H</i>	29.1	70.8	0.1
<i>K</i>	16.0	83.9	0.1

Table 1. Weight (in %) of stellar radiation, nebular continuum and emission lines at various wavelengths at initial time for an instantaneous burst.

3.1.3. The inner part of elliptical galaxies

The E1 template, characterizing the metal-rich inner part of ellipticals, compiled by Arimoto (1996) from the data of Bica (1988), Burstein et al. (1988) and Persson et al. (1979), is well fitted on Fig. 5 by a 17-Gyr-old burst model

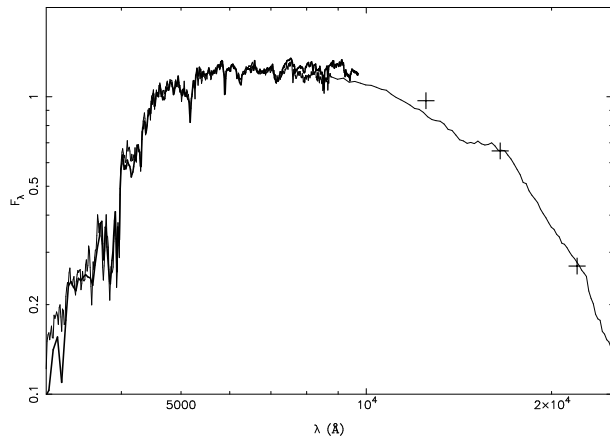


Fig. 5. Comparison of a 17-Gyr-old instantaneous burst (thin) with the E1 spectrum built by Arimoto (1996) (thick line and crosses) from various sources.

from the *U* to the *K*. Though slightly deficient, the predicted flux in the *J*-band at solar metallicity is notably better than in previous models of ellipticals, as noted by Arimoto (1996). The reason is likely the careful calibration of stellar spectra and colors between the *J* and *K* bands. The E1 template shows a steep UV upturn in the far UV, due presumably to old metal-rich stars of which discussion is beyond the scope of this paper. Its metallicity is therefore very likely higher than solar as in the central part of typical giant ellipticals (Munn 1992). Because of the age-metallicity degeneracy in the optical-NIR (Worthey 1994), the best-fitting age of 17 Gyr obtained with the solar metallicity model is thus only an upper limit. Integrated spectra on the whole galaxy of spheroidal galaxies are however bluer in the optical-NIR and have a mean lower metallicity than the core (Munn 1992), allowing us to fit them at the younger age of 13 Gyr (see 3.2.1).

The general agreement of the E1 template with our burst spectrum makes us confident for using our model to build various scenarios of evolution and a new atlas of synthetic spectra (see Rocca-Volmerange & Fioc (1996), in Leitherer et al. (1996b)). Timescales and resolution allow to simulate starbursts as well as evolved galaxies.

3.2. Galaxies of the Hubble sequence

Normal galaxies are the sum of stellar populations of different ages, well simulated with our basic instantaneous starburst. Because of the insufficient knowledge of star formation physics, we prefer to follow the classical hypothesis of an SFR law $\tau(t)$ depending on the gas fraction g by $\tau(t) = \nu g(t)$ and to explore the values of the astration rate ν leading to best fits of Hubble sequence galaxies.

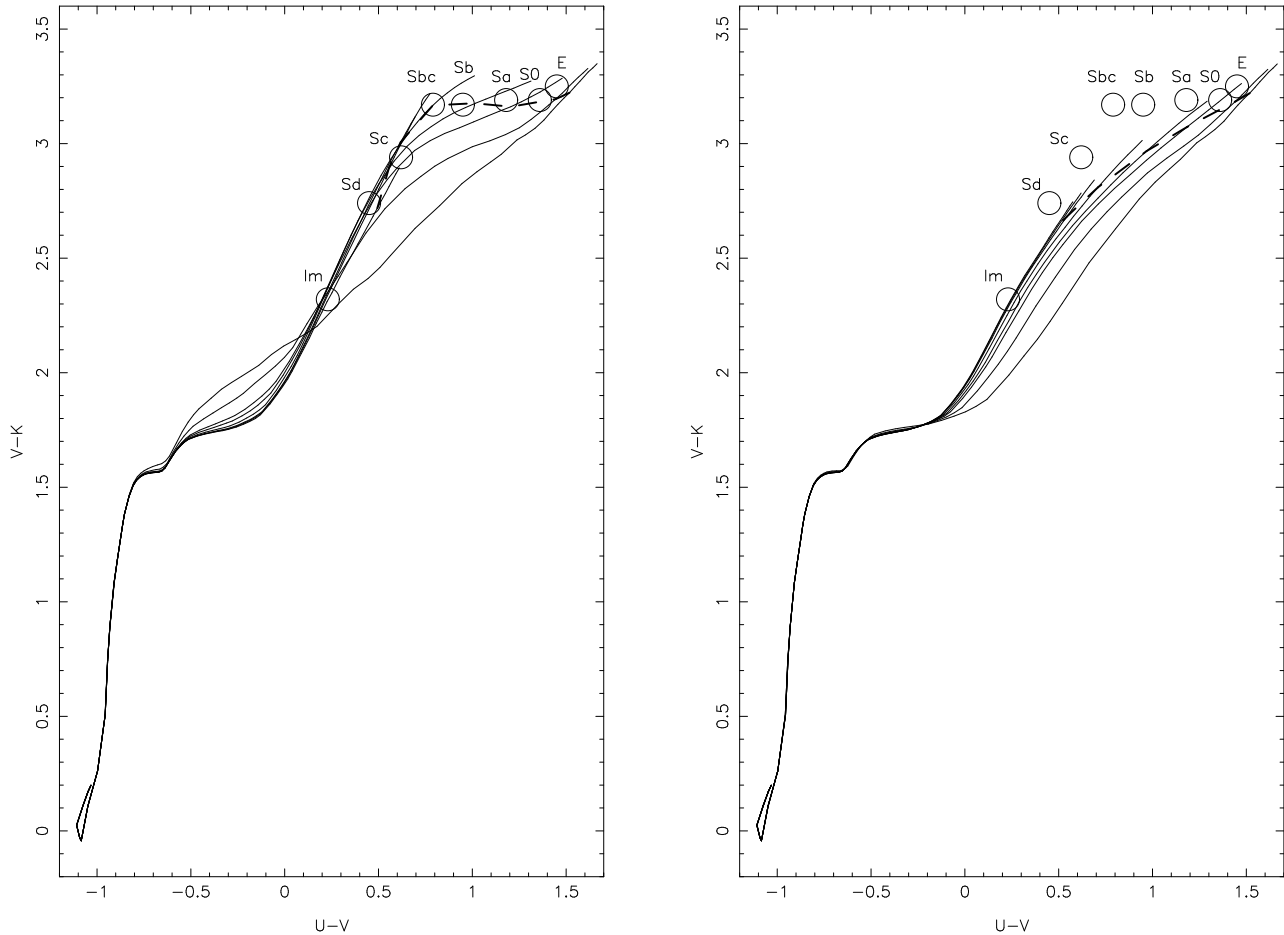


Fig. 6. Left: color evolution (solid) of the synthetic spectra for various star formation histories in the $(U - V, V - K)$ diagram. The dashed line corresponds to 13 Gyr-old galaxies. Extinction and nebular emission are considered. Right: the same without extinction. Circles are the data as in Aaronson (1978).

3.2.1. Optical-NIR colors

Spectral templates observed through large apertures for each Hubble type are needed for high-redshift predictions. The literature has essentially published spectra obtained through small apertures (Kinney et al. 1996) or limited to the optical wavelength range (Kennicutt 1992). Thus, we are limited to use statistical samples of colors. A coherent set of optical-NIR colors of nearby galaxies related to morphological type have been obtained by Aaronson (1978) (including Huchra (1977) data) for an aperture $\log_{10}(A/D_0) = -0.2$. We plot on Fig. 6 the time evolution of $U - V$ and $V - K$ colors for scenarios fitting the observed colors. An inclination of 1 rad, which is the mean inclination integrated over solid angles, is assumed for spiral galaxies. Ages of about 13 ± 2 Gyr are obtained for giant spirals (Sa-Sc). Neglecting the effect of extinction would lead to excessive ages, as shown by Fig. 6. The $(U - V, V - K)$ diagram shows a strong degeneracy for late

spirals. The confusion of curves corresponding to slowly-evolving SFR in this region allows a large interval of ages for these galaxies. Maximal age solutions are obtained for 10 Gyr-old Sd and 4-5 Gyr-old Im. If we assume an increasing SFR, very similar colors may however be obtained at 10 Gyr for Im.

However, for early-type galaxies, a gas-dependent SFR in a closed-box model with constant IMF would lead to an excessive residual current star formation and too blue colors, whatever the star formation law may be. Indeed, if the bulk of the stars formed very early, the mass ejection of old stars $r_{\text{old}}(t)$ will depend mainly on age and not on the detailed star formation history. In the hypothesis of some residual star formation, high-mass stars which have just formed and died in releasing large amounts of gas will also contribute to the gas content. This component is proportional to the current SFR and may be written $\tau(t)r_{\text{young}}$. The classical equation of evolution of the gas fraction in

a closed model leads with previous approximations, for a decreasing gas fraction, to

$$\frac{dg}{dt} \simeq -\tau(t) + r_{\text{old}}(t) + \tau(t)r_{\text{young}} \leq 0$$

and we finally get

$$\tau(t) \geq \frac{r_{\text{old}}(t)}{1 - r_{\text{young}}}.$$

The resulting minimal SFR gives excessively blue $U - V$ (1.35 at 16 Gyr) and, even more importantly, UV colors. A possible star formation must thus be quenched to recover the colors of normal spheroidal galaxies. However, the gas ejected by old low-mass stars alone since the age of 1 Gyr amounts to nearly 10% of the mass, depending slightly on the IMF, anyway much more than observed (Faber & Gallagher 1976). The fate of this gas is unclear and a dynamical model would be required to determine it, which is beyond the scope of this model. For this reason, we simply assume the following star formation law: $\tau(t) = \eta\nu g(t)$, where $\eta = g(t)/(g(t) + g_c)$ and g_c is a threshold that we conveniently take equal to 0.01; η is nearly equal to 1 at high gas fraction and decreases rapidly to 0 when gas rarefies, suppressing star formation. The remainder $((1 - \eta)\nu g)$ is assumed to be expelled by late galactic winds induced by SNIa in a low-density environment or locked in the formation of very low-mass stars. By relaxing the hypotheses of a closed box or constant IMF, we obtain reasonable colors for E/S0.

Our sequence of galaxy colors also compares favorably with the Bershady (1995) data (see Fig. 7). Although the dispersion is due partly to photometric uncertainties, extinction effects (inclination) and irregular star formation histories are certainly also important. The slightly bluer $U - J$ of the Bershady (1995) data relative to our synthetic galaxies may be due to the fact that Bershady (1995) magnitudes are computed over the whole galaxy, whereas those of Aaronson (1978) are given for an aperture of $\log_{10}(A/D_0) = -0.2$. We prefer however to keep the Aaronson (1978) values, because Bershady (1995) does not give a correspondence with morphological type that we need for galaxy counts.

The $B - V$ color may finally be compared with the mean values of RC3 published by Buta et al. (1994) to check that the identifications of the morphological types of Aaronson (1978) are correct. Since these are face-on corrected values, we correct spiral RC3 colors to an inclination of 1 rad corresponding to a value of $\log_{10} R_{25} \sim 0.25$ and gather RC3 types to agree with our types when necessary. Differences never exceed 0.05 mag.

The characteristics and the main colors of the computed spectra as well as the RC3 values are given in Table 2.

3.2.2. Optical spectra

We may compare our spectra in the optical range with those of Kennicutt (1992). Our spectral continua are in very close agreement with that sample (Fig. 8), after correction for redshift and deletion of emission lines by Galaz & de Lapparent (1996). In particular, typical features such as the Balmer jump and the MgI and TiO lines are surprisingly well reproduced.

4. Calibration of bright counts

Because they do not depend on the cosmological parameters, bright galaxy counts ($15 < b_j < 19$) are a straightforward constraint on spectral evolution models and notably on the reliability of the $z = 0$ templates. Two related problems concerning bright counts arose in previous analyses (Guiderdoni & Rocca-Volmerange 1990; Pozzetti et al. 1996), namely the slope at bright magnitudes and the normalization of the luminosity function. Maddox et al. (1990) have found in the APM survey a steeper slope of number counts between $b_j = 15$ and $b_j = 19$ than allowed by pure luminosity evolution models, implying a much more rapid evolution at low redshift. As a result, when model predictions are calibrated on observed counts in the brightest bins, a strong deficit of predicted counts relative to observed ones is obtained at faint blue magnitudes. Although the corresponding low normalization of the luminosity function is in agreement with Loveday et al. (1992), most models have preferred until now to normalize the counts at fainter magnitudes ($b_j \sim 19$), where evolution may become non-negligible, to recover agreement with faint counts.

This is clearly a crucial problem for the reliability of evolution models. However, recent observational results do not confirm the conclusions of Maddox et al. (1990). The re-analysis of the photometry of APM data by Metcalfe et al. (1995) and the counts of Bertin & Dennefeld (1996) favor a flatter slope and a high normalization of the luminosity function. To clarify this controversy, a multispectral analysis of bright counts is needed, highlighting by different weights of old and young stellar populations in the various bands, whether a strong evolution has happened recently or not. The NIR, in particular, is dominated by slowly-evolving old stellar populations and should therefore be more sensitive to number density evolution than to recent star formation. Moreover, in this wavelength range, the k-corrections for different types are very similar, contrary to the UV. Finally, it is less affected than the blue by the uncertainties in the luminosity functions of late-type galaxies. For these reasons, predictions in the K -band are more reliable than at shorter wavelengths. The evolutionary spectra built by PEGASE are particularly useful for this purpose, thanks to their large continuous range of wavelength and valid fits of nearby observational templates.

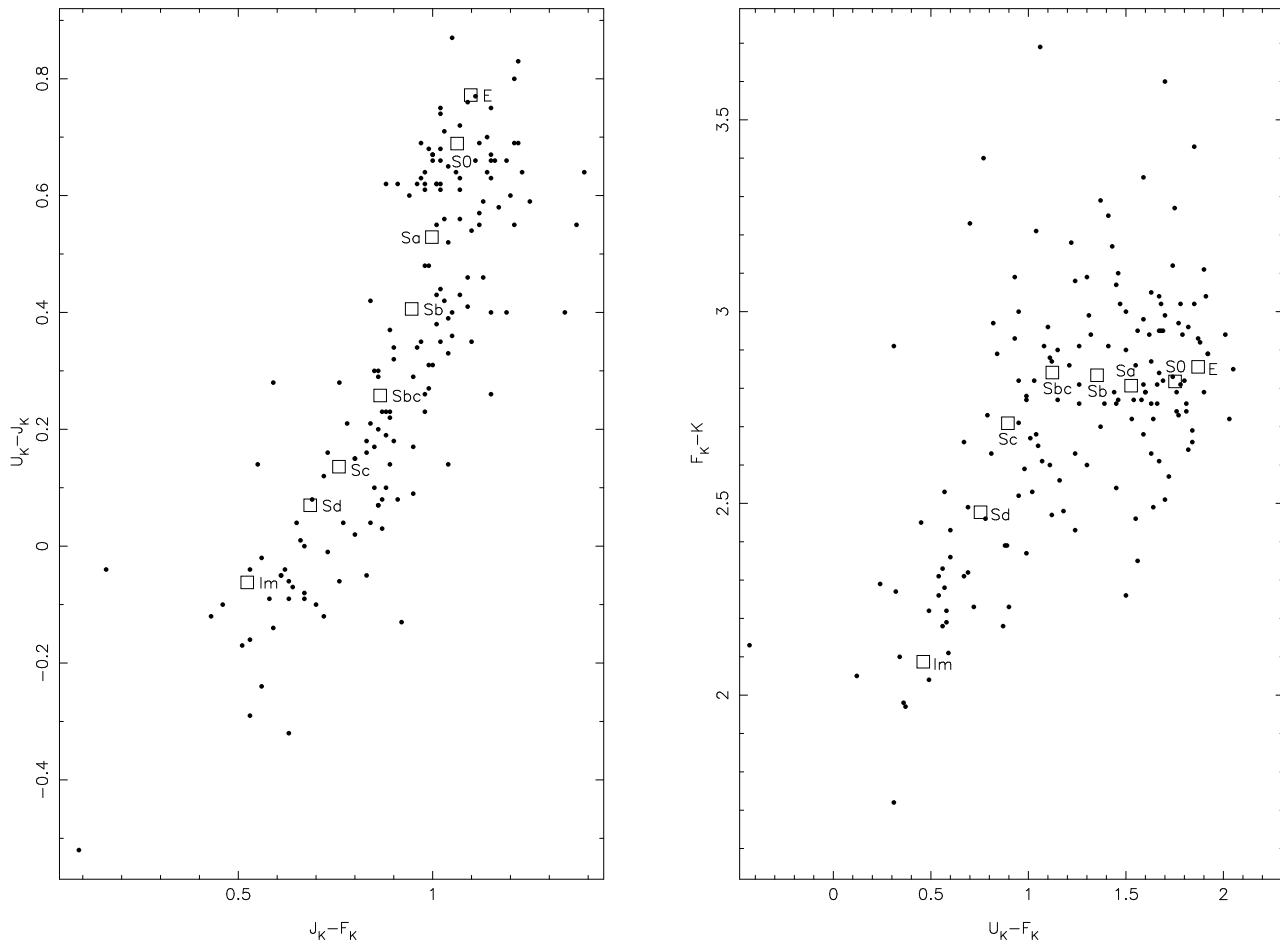


Fig. 7. Comparison to Bershadsky (1995) data (dots). U , J and F are the photographic bands of Koo (1980) and Kron (1986). Left: $(U - J, J - F)$ diagram. Right: $(U - F, F - K)$ diagram. Squares are our synthetic templates at $z = 0$.

Model type	E	S0	Sa	Sb	Sbc	Sc	Sd	Im
RC3 types	-5,-4	-3,-2,-1	0,1	2,3	4	5	6,7,8	9,10
ν ($10^{-3} M_{\odot} \cdot \text{Myr}^{-1}$)	2	1	0.5	0.35	0.2	0.1	0.07	0.05
age (Gyr)	13	13	13	13	13	12	10	4.5
$(B - V)_{\text{RC3}}$	0.91	0.90	0.83	0.75	0.65	0.59	0.50	0.44
$B - V$	0.95	0.92	0.84	0.78	0.69	0.59	0.53	0.39
$U - B$	0.57	0.51	0.34	0.23	0.09	0.00	-0.06	-0.16
$V - K$	3.23	3.19	3.16	3.18	3.17	2.96	2.75	2.31
$V - R_c$	0.61	0.59	0.57	0.56	0.54	0.49	0.45	0.36
$V - I_c$	1.26	1.24	1.21	1.20	1.16	1.06	0.97	0.78
$J - H$	0.75	0.75	0.75	0.76	0.77	0.75	0.71	0.64
$H - K$	0.18	0.18	0.18	0.19	0.20	0.19	0.17	0.15
M/L_B ($M_{\odot}/L_{B_{\odot}}$)	6.92	6.15	5.02	4.60	4.25	3.87	3.74	3.67

Table 2. Evolutionary parameters and colors of the synthetic templates.

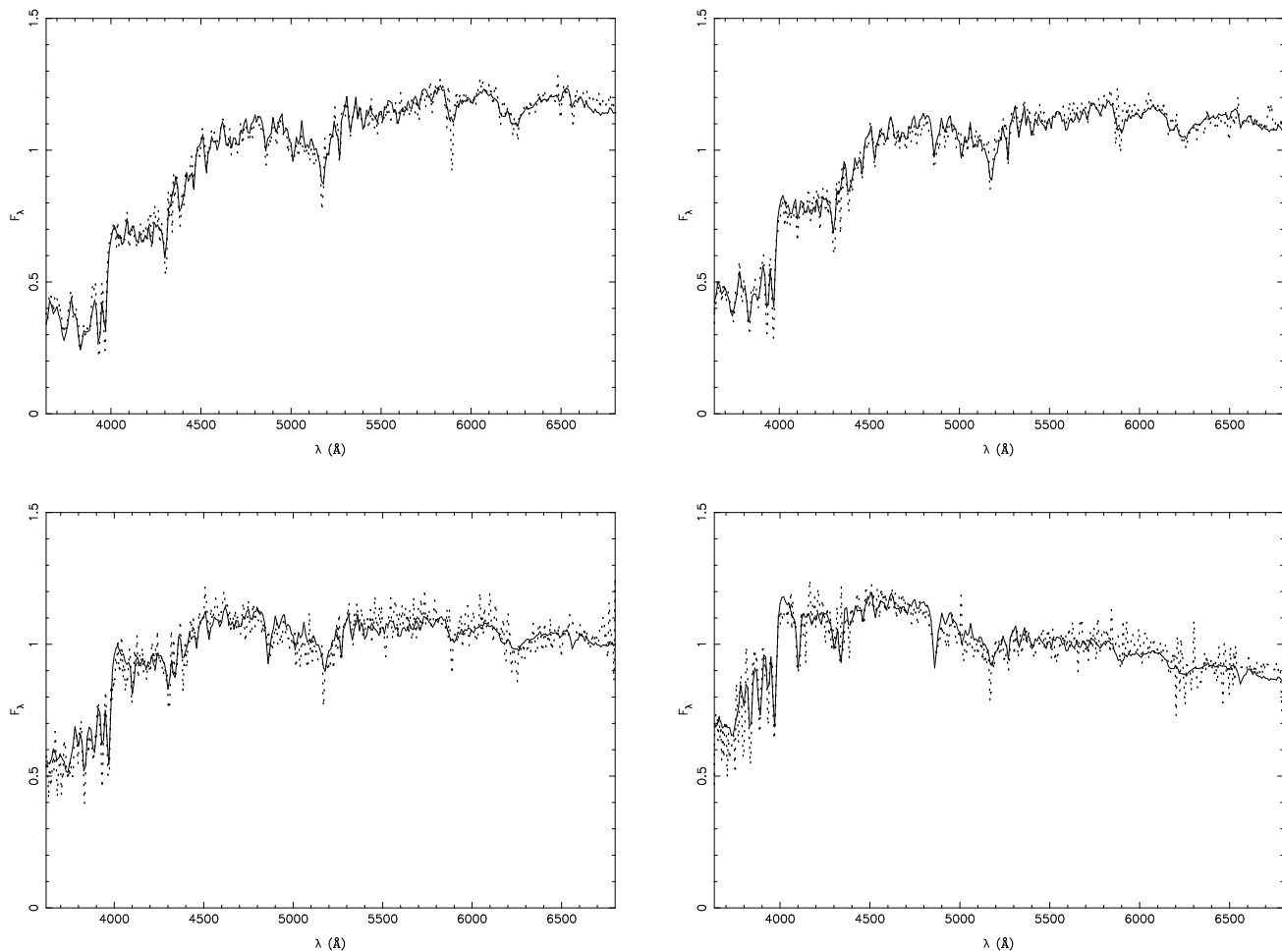


Fig. 8. Comparison of our synthetic spectra at $z = 0$ (solid) to Kennicutt (1992) spectra (dotted). Top left: synthetic elliptical vs. NGC 3379 (RC3 type=-5). Top right: synthetic Sa vs. NGC 3368 (RC3 type=2). Bottom left: synthetic Sbc vs. NGC 3147 (RC3 type=4). Bottom right: synthetic Sd vs. NGC 6643 (RC3 type=5).

We have modelled galaxy counts in the 3 bands b_j , I and K (Fig. 9). The adopted luminosity function is that of Marzke et al. (1994), after correction of the Zwicky magnitudes M_Z^* by $B^* - M_Z^* = -0.29$, the mean value obtained by Efstathiou et al. (1988), to convert them in B magnitudes. Characteristics of the luminosity functions are given in Table 3. When necessary, we redistribute the types given for the LF in our standard types. We take $H_0 = 65 \text{ km.s}^{-1}.\text{Mpc}^{-1}$ in agreement with Tanvir et al. (1995). An open cosmology ($q_0 = 0.05$, $\Lambda_0 = 0$) is assumed, leading to an age of the universe of 13.5 Gyr greater than the age of our older standard galaxies, but does not in any way affect the simulation of bright counts. Redshifts of formation in this cosmology (see Table 3) are taken in agreement, within the uncertainties, with the ages of the reference model spectra. We finally normalize our counts on Bertin & Dennefeld (1996) counts at $b_j = 16$.

We obtain good agreement with Gardner et al. (1996) *multispectral* bright counts in the 3 bands b_j , I and K for the same value of normalization, confirming that the evolution scenarios and colors of the galaxies dominating bright counts are correct. Moreover, the value of $\phi^* = 23.8 \cdot 10^{-3} h^3 \text{ Mpc}^{-3}$ from modeling is fully consistent with the normalization $(20.1 \pm 5.0) \cdot 10^{-3} h^3 \text{ Mpc}^{-3}$ of the Marzke et al. (1994) luminosity function that we use.

Predictions at fainter magnitudes in various cosmologies and constraints from redshift and color distributions as well as correlation functions will be extensively discussed in a future paper.

5. Discussion and conclusion

The understanding of galaxy evolution requires models of spectral evolution. The model proposed here benefits from many improvements and new input data, in particular in the NIR. It becomes sufficiently reliable to be entirely pub-

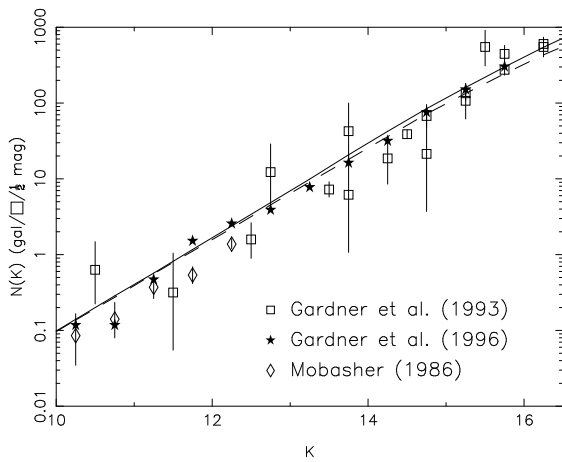
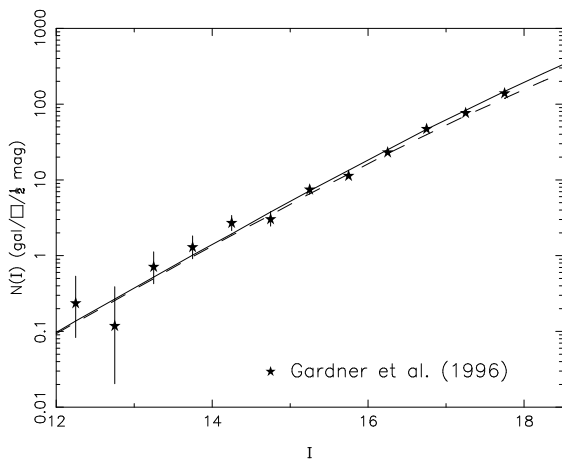
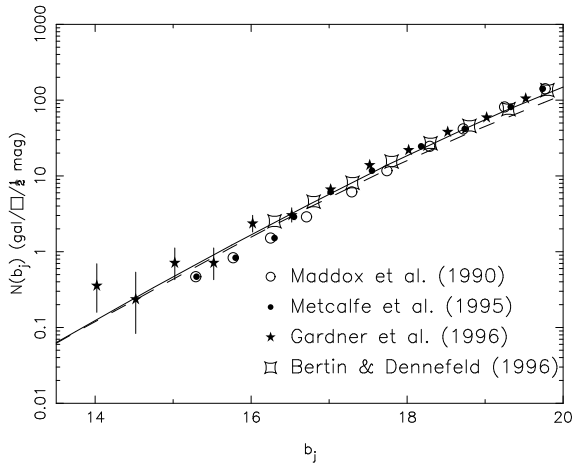


Fig. 9. Galaxy counts in b_j , I and K with the Marzke et al. (1994) luminosity function. Cosmological parameters are $H_0 = 65 \text{ km.s}^{-1}.\text{Mpc}^{-3}$, $q_0 = 0.05$ and $\Lambda_0 = 0$. The solid (resp. dashed) lines are our predicted counts with (resp. without) evolution.

Type	z_i^{for}	B_i^*	α_i	$g_i = \phi_i^* / \sum \phi_i^*$
E	20	-19.52	-0.85	0.066
S0	20	-19.03	-0.94	0.250
Sa	5	-19.03	-0.94	0.083
		-19.01	-0.58	0.095
Sb	5	-19.01	-0.58	0.191
Sbc	5	-19.01	-0.58	0.096
Sc	5	-19.10	-0.96	0.064
Sd	2	-19.10	-0.96	0.129
Im	0.5	-19.08	-1.87	0.026

Table 3. Redshifts of formation and luminosity functions (Schechter parametrization) of our standard synthetic spectra. B^* is given for $H_0 = 100 \text{ km.s}^{-1}.\text{Mpc}^{-1}$. Two LFs are given for Sa and should be added. The reason for this is that the S0 type of Marzke et al. (1994) includes S0/a, while these are included in our synthetic Sa. Part of the S0 LF is for this reason transferred to the synthetic Sa.

lished as a useful tool for many evolution studies. The wide wavelength range ($220 \text{ \AA} - 5 \mu\text{m}$) of the library of stellar spectra and the capacity of the algorithm to follow the evolution on very rapid (1 Myr) and very long timescales (20 Gyr) provide constraints on the weights of various stellar populations in starbursts and evolved galaxies. The inclusion of extinction, notably in E/S0, and nebular emission has been attempted in consistency with the evolution of stars. A library of standard synthetic evolving spectra has been built and shows a fair agreement with $z = 0$ galaxies from observed optical spectra and colors in the near-UV, optical and NIR. Several samples of templates are used to define a set of reference synthetic spectra at $z = 0$, adopted as typical of 8 spectral types of the Hubble sequence. An age of about 13 Gyr is derived from optical-NIR colors for spheroidals and early spirals and decreases for later types.

Predicted galaxy counts agree with most recent optical and NIR bright counts as well as with new determinations of the normalization of the luminosity function, confirming that the evolution of nearby galaxies is well described by pure luminosity evolution models.

Uncertainties in the stellar evolutionary tracks are discussed in this paper, and we tried to reduce at maximum those related to stellar atmospheres. Other main uncertainties concern the effects of extinction and metallicity. The optical thickness of spirals, as well as the state of the ISM and the resulting extinction in ellipticals, are still a matter of debate. The influence of the metallicity on extinction curves, stellar spectra and evolutionary tracks could be important in metal-rich ellipticals as well as metal-poor H II galaxies. Finally, the star formation (SFR, IMF) in galaxies should be derived from a chemodynamical model.

In spite of these uncertainties, this model should prove useful to the astronomical community. The code sources,

input data, especially our selected stellar library², and the atlas of evolving synthetic spectra of standard galaxies (spectra, colors, equivalent widths of emission lines, numbers of SNII) with corresponding k- and e-corrections are available on an AAS CD-ROM (see Fioc & Rocca-Volmerange (1996) and Rocca-Volmerange & Fioc (1996) in Leitherer et al. (1996b)) and the latest version corresponding to this paper may be obtained at addresses given in the abstract. It may be easily used by anyone, even unfamiliar with spectral evolution questions, but also, thanks to its structure, adapted by those interested in this subject. We hope to allow fruitful comparisons with other existing models. Further improvements will also be available by ftp. Comments, questions and suggestions may be sent to *pegase@iap.fr*.

References

- Aaronson M. 1978, ApJ 221, L103
Arimoto N. 1996, in: From Stars to Galaxies: the Impact of Stellar Physics on Galaxy Evolution, Leitherer C., Fritze-v. Alvensleben U., Huchra J. (eds.), ASP Conference Series, Vol. 98, p. 287
Bershady M.A. 1995a, AJ 109, 87
Bertelli G., Bressan A., Chiosi C., Fagotto F., Nasi E. 1994, A&AS 106,275
Bertin E., Dennefeld M. 1996, A&A (in press)
Bessel M.S. 1995, in: The Bottom of the Main Sequence – and beyond, Tinney C.G. (ed.), Springer-Verlag, p. 123
Bessel M.S., Brett J. 1988, PASP 100, 1134
Bica E. 1988, A&A 195, 76
Blöcker T. 1995, A&A 299, 755
Bressan A., Fagotto F., Bertelli G., Chiosi C. 1993, A&AS 100, 647
Broadhurst T.J., Ellis R.S., Glazebrook K. 1992, Nature 355, 55
Brown R.L., Mathews W.G. 1970, ApJ 160, 939
Bruzual G., Charlot S. 1997 (in preparation)
Buat V., Donas J., Deharveng J.M. 1987, A&A 185, 33
Burstein D., Bertola F., Buson L.M., Faber S.M., Lauer T.R. 1988, ApJ 328, 440
Buta R., Mitra S., de Vaucouleurs G., Corwin H.G. Jr. 1995, AJ 107, 118
Calzetti D., Kinney A.L., Storchi-Bergmann T. 1994, ApJ 429, 582
Charbonnel C., Meynet G., Maeder A., Schaerer D. 1996 A&AS 115, 339
Charlot S., Worthey G., Bressan A. 1996, ApJ 457, 625
Charlot S. 1996, in: From Stars to Galaxies: the Impact of Stellar Physics on Galaxy Evolution, Leitherer C., Fritze-v. Alvensleben U., Huchra J. (eds.), ASP Conference Series, Vol. 98, p. 275
Charlot S., Bruzual A.G. 1991, ApJ 367, 126
Chiosi C. 1986, in: Spectral evolution of galaxies, Dordrecht, D. Reidel Publishing Co., 1986, p. 237
Clegg R.E.S., Middlemass D. 1987, MNRAS 228, 759
DeGioia-Eastwood K. 1992, ApJ 397, 542
Efstathiou G., Ellis R.S., Peterson B.A. 1988, MNRAS 232, 431
Engelke C.W. 1992, AJ 104, 1248
Faber S.M., Gallagher J.S. 1976, ApJ 204, 365
Ferland G.J. 1980, PASP 92, 596
Ferland G.J. 1995 (private communication)
Fluks M.A., Plez B., Thé P.S., de Winter D., Westerlund B., Steenman H.C. 1994, A&AS 105, 311
Fröhlich H.-E. 1982, AN 303, 97
Fukugita M., Yamashita K., Takahara F., Yoshii Y. 1990, ApJ 361, L1
Galaz G., de Lapparent V. 1997 (in preparation)
Gardner J.P., Cowie L.L., Wainscoat R.J. 1993, ApJ 415, L9
Gardner J.P., Sharples R.M., Carrasco B.E., Frenk C.S. 1996, MNRAS 282, L1
Giles K. 1977, MNRAS 180, 57
Groenewegen M.A.T., de Jong T. 1993, A&A 267, 410
Guiderdoni B., Rocca-Volmerange B. 1987, A&A 186, 1
Guiderdoni B., Rocca-Volmerange B. 1990, A&A 227, 362
Gunn J.E., Stryker L.L. 1983, ApJS 52, 51
Heck A., Egret D., Jashek M., Jashek C. 1984, A&AS 57, 213
Huchra J.P. 1977, ApJS 35, 171
Iglesias C.A., Rogers F.J., Wilson B.G. 1992, ApJ 397, 717
Jacoby G.H., Hunter D.A., Christian C.A. 1984, ApJS56, 257
Kennicutt R.C. 1992, ApJS 79, 255
Kinney A.L., Calzetti D., Bohlin R.C., McQuade K., Storchi-Bergmann T., Schmitt H.R. 1996, ApJ 467, 38
Koo D.C. 1986, ApJ 311, 651
Kron R.G. 1980, ApJS 43, 305
Kurucz R.L. 1992, in: The stellar populations of galaxies (IAU Symp. 149), Barbuy B., Renzini A. (eds.), Dordrecht, Kluwer
Lançon A., Rocca-Volmerange B. 1992, A&AS 96, 593
Lançon B., Rocca-Volmerange B. 1996, New Astronomy 1, 215
Lanz T. 1986, A&AS 65, 195
Leitherer C., Fritze-v. Alvensleben U., Huchra J. (eds.) 1996a, From Stars to Galaxies: the Impact of Stellar Physics on Galaxy Evolution ASP Conference Series, Vol. 98
Leitherer C., Alloin D., Fritze-v. Alvensleben U., Gallagher J.S., Huchra J.P., Matteucci F., O’Connell R.W., Beckman J.E., Bertelli G., Bica E., Boisson C., Bonatto C., Bothun B., Bressan A., Brodie J.P., Bruzual G., Burstein D., Buser R., Caldwell N., Casuso E., Cerviño M., Charlot S., Chavez M., Chiosi C., Christian C.A., Cuisinier F., Dallier R., de Koter A., Delisle S., Díaz A.I., Dopita M.A., Dorman B., Fagotto F., Fanelli M.N., Fioc M., García-Vargas M.L., Girardi L., Goldader J.D., Hardy E., Heckman T.M., Iglesias J., Jablonka P., Joly M., Jones L., Kurth O., Lançon A., Lejeune T., Maeder A., Malagnini M.A., Marigo P., Mas-Hesse J.M., Meynet G., Möller C.S., Mollá M.L., Morossi C., Nasi E., Nichols J.S., Ødegaard K.J.R., Parker J.W., Pastoriza M.G., Peletier R., Robert C., Rocca-Volmerange B., Schaerer D., Schmidt A., Schmitt H.R., Schommer R.A., Schmutz W., Serote Roos M., Silva L., Stasińska G., Sutherland R.S., Tantaló R., Traat P., Vallenari A., Vazdekis A., Walborn N.R., Worthey G.S., Wu C.-C. 1996b, PASP 108, 996 (AAS CD-ROM Series, Vol. 7)
Loveday J., Peterson B.A., Efstathiou G., Maddox S.J. 1992, ApJ 390, 338
Maddox S.J., Sutherland W.J., Efstathiou G., Loveday J., Peterson B.A. 1990, MNRAS 241, 1p

² We also propose another library of intermediate resolution (1.4 Å) optical stellar spectra selected from Jacoby et al. (1984).

- Maeder A., Meynet G. 1989, *A&A* 210, 155
- Marzke R.O., Geller M.J., Huchra J.P. Corwin H.G. 1994, *AJ* 108, 437
- Metcalfe N., Fong R., Shanks T. 1995, *MNRAS* 274, 769
- Mobasher B., Ellis R.S., Sharples R.M. 1986, *MNRAS* 223, 11
- Munn J.A. 1992, *ApJ* 399, 444
- Natta A., Panagia N. 1984, *ApJ* 287, 228
- Osterbrock D.E. 1989, *Astrophysics of Gaseous Nebulae and Active Galactic Nuclei*, University Science Books
- Pengelly R.M. 1963, *MNRAS* 127, 145
- Persson S.E., Frogel J.A., Aaronson M. 1979, *ApJS* 39, 61
- Pozzetti L., Bruzual A.G., Zamorani G. 1996, *MNRAS* 281, 953
- Rana N.C., Basu S. 1992, *A&A* 265, 499
- Rocca-Volmerange B., Guiderdoni B. 1988, *A&AS* 75, 93
- Rocca-Volmerange B., Guiderdoni B. 1990, *MNRAS* 247, 166
- Savage B.D., Mathis J.S. 1979, *ARA&A* 17, 73
- Schaller G., Schaerer D., Meynet G., Maeder A. 1992, *A&AS* 96, 269
- Schönberner D. 1983, *ApJ* 272, 708
- Searle L., Sargent W.L.W., Bagnuolo W.G. 1973, *ApJ* 179, 427
- Silva D.R., Wise M.W. 1996, *ApJ* 457, L15
- Spinoglio L., Malkan M.A. 1992, *ApJ* 399, 504
- Straižys, V. 1992, *Multicolor stellar photometry*, Pachart, Tucson (Astronomy and Astrophysics Series 15)
- Tanvir N.R., Shanks T., Ferguson H.C., Robinson D.R.T. 1995, *Nature* 377, 27
- Timmes F.X., Woosley S.E., Weaver T.A. 1995, *ApJS* 98, 617
- Tinsley B.M. 1972, *A&A* 20, 383
- Tsai J.C., Mathews W.G. 1995, *ApJ* 448, 84
- Tylenda R., Stasińska G. 1994, *A&A* 288, 897
- Vacca W.D., Garmany C.D., Shull J.M. 1996, *ApJ* 460, 914
- Vandenbergh D.A., Hartwick F.D.A., Dawson P. 1983, *ApJ* 266, 747
- Vassiliadis E., Wood P.R. 1993, *ApJ* 413, 641
- Wang B., Heckman T.M. 1996, *ApJ* 457, 645
- Wesselius P.R., Van Duinen R.J., de Jonge A.R.W., Aalders J.W., Luinge W., Wildeman K.J. 1982, *A&AS* 49, 427
- Wise M.W., Silva D.R. 1996, *ApJ* 461, 155
- Witt A.N., Thronson H.A., Capuano M.Jr. 1992, *ApJ* 393, 611
- Woosley S.E., Weaver T.A. 1995, *ApJS* 101, 181
- Worthey G. 1994, *ApJS* 95, 107
- Yoshii Y., Takahara F. 1988, *ApJ* 326, 1